VALIDATION OF AERODYNAMIC AND AEROACOUSTIC COMPUTATIONS OF A FENESTRON® IN REAL FLIGHT CONDITIONS[†]

P. GARDAREIN
ONERA (DAAP/H2T)
8 rue des Vertugadins
FR-92190 Meudon

F. FALISSARD[‡]
ONERA (DSNA/ACOU)
29 av. de la Division Leclerc
FR-92320 Châtillon

L. BINET
ONERA (DCSD/PSEV)
Base Aérienne 701
FR-13661 Salon de Provence

J.-C. CAMUS
DGA Essais en vol
Base d'essais d'Istres
FR-13128 Istres Air

Abstract

This paper presents the validation of aerodynamic and aeroacoustic computations of a Fenestron® fan-in-fin tail rotor against aerodynamic and acoustic flight test measurements. Comparisons are presented for two flight conditions: a takeoff at 75kt with high climb rate and a level flight at 150 kt. For both flight conditions, computed and measured unsteady blade pressures are in good agreement even if the computation tends to overestimate the unsteady pressure fluctuation. Comparison of measured and computed acoustic spectra at microphone locations exhibit similar shapes with a better agreement for the takeoff flight condition than for the level flight condition.

Introduction

The enhancement of numerical tools used for quiet helicopter studies has yield a lot of progress in predicting main rotor impulsive noise. However, the main rotor is not the only noise source of a helicopter. In some flight conditions, the tail rotor plays a significant part in the helicopter acoustic nuisance and has to be considered in the design of low-noise flight procedures. The flow field occurring in a shrouded tail rotor such as the Eurocopter Fenestron® is very complex and depends strongly on the flight parameters so that noise predictions cannot be performed by using analytical models. In this case, CFD is required for providing input data to aeroacoustic integral methods.

In this context a specific study has been launched by ONERA and Eurocopter with support of the French Ministry of Civil Aviation (DGAC), first to acquire an experimental comprehensive data base dedicated to Fenestron® noise analysis, secondly to develop aerodynamic and aeroacoustic simulation tools sufficiently accurate for Fenestron® noise prediction and to compare computational results against the experiments. The first aerodynamic and aeroacoustic computations of a Fenestron® in flight conditions [1, 2], respectively based on the Unsteady Reynolds-Averaged Navier-Stokes (URANS) equations and the Ffowcs Williams-Hawkings equation, have proven the capability of the numerical tools to capture the main aerodynamic and aeroacoustic features of the Fenestron®. In order to validate the numerical computations against relevant experimental data, the Dauphin 6075 helicopter of the DGA Flight Test Center has been specifically instrumented [3, 4]. Flight tests have been carried out to build up an experimental data base that has already been used to perform aerodynamic and acoustic analysis of the Fenestron characteristics depending on the flight conditions [5, 6].

This paper addresses the first comparisons of aerodynamic and aeroacoustic computations against the experimental data obtained during the Fenestron® noise flight test campaign. It is organized as follows. The experimental setup is first presented, which consists in the Dauphin 6075 research helicopter, the test program, the instrumentation and the data processing. Then both numerical methods and setups used for aerodynamic and aeroacoustic computations are detailed. The last part of this paper is dedicated to the comparison of numerical results and real flight data for a selected flight condition.

[†] Presented at the 36th European Rotorcraft Forum, Paris, France, September 7-9, 2010

[‡] Corresponding author: Fabrice.Falissard@onera.fr

1 Flight test data

1.1 Dauphin 6075 setup

The Dauphin 6075 used for the flight tests is an Eurocopter SA365N helicopter equipped with a Fenestron® of first generation. It is composed by a rotor with 13 equally spaced blades mounted on a hub supported by 3 equally spaced arms [7]. The shroud diameter is 0.9 m and the nominal rotation speed is about 4700 rpm which corresponds to a blade passing frequency (BPF) of about 1 kHz. Although this rather old and simple geometry is not representative of modern Fenestron® with uneven blade spacing out of acoustic concerns [8, 9, 10, 11, 12], its use is interesting for physical insight and validation of the aerodynamic and aeroacoustic computation tools which are the purposes of this study. Moreover, this Fenestron has been previously identified as a non negligible source of the noise radiated by the Dauphin 6075 helicopter depending on the flight conditions [13, 14].

Figure 1: Microphone locations on the Dauphin 6075 for acoustic measurements

1.2 Instrumentation

The development, integration and testing of the innovative instrumentation used for the in-flight measurements is fully described in [3, 4, 6]. This instrumentation consists in two distinct parts, one fixed on the fuselage and one rotating with the tail rotor. The fixed part is composed of steady wall pressure sensors on the rear part of the fuselage and tail, of steady and unsteady wall pressure sensors in the Fenestron® duct, of Pitot probe rakes in the duct and microphones fixed on the horizontal empennage. These measurement devices are shown in figures 1 and 2. The rotating part of the instrumentation consists in a trigger system, in pairs of upper/lower thin layer unsteady Kulite pressure transducers mounted on 4 blades of the Fenestron® at 0.7 radius and in strain gauges fixed on a reference blade, all displayed in figure 2.

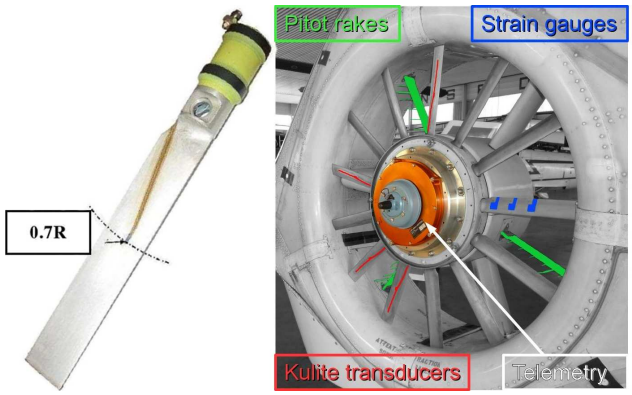

Figure 2: Instrumented blade, rotor and duct for Fenestron® aerodynamic measurements

1.3 Flight test program

The flight tests, carried out by the DGA Flight Test crew from November 2008 to January 2009, consists in many stabilized flight conditions: take-offs, approaches, level flights and side-slip flights. As shown in figure 3, the flight speeds vary between 50 and 150 kt with climb or descent angles varying between +2000 and -2000 ft/mn.

1.4 Data processing

Each flight was recorded continuously so that the stabilized flight phases corresponding to the test program were first extracted from the recordings by the DGA Flight Test Center. Using the calibration of the different sensors and instrumentation chains, these experimental data were then converted into physical units by ONERA's Systems Control and Flight Dynamics Department (DCSD) and sent to the Applied Aerodynamics Department (DAAP) and to the Computational Fluid Dynamics and Aeroacoustics Department (DSNA) for

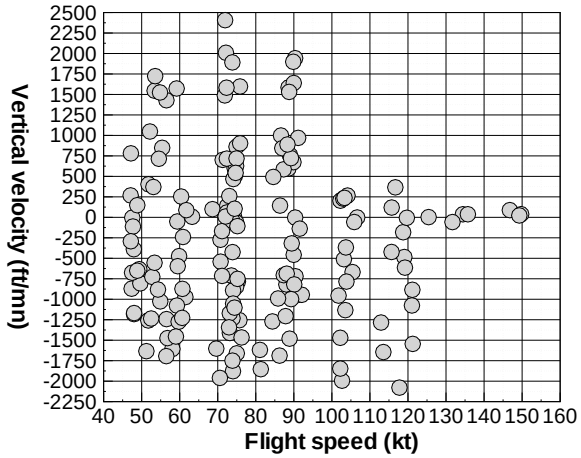

Figure 3: Flight conditions measured during the Fenestron® flight tests

exploitation and analysis. For each track corresponding to a flight case, the unsteady data have been processed on an interval selected in order to minimize the variations of the flight parameters such as flight velocity, climb or descent rate and side-slip angle.

The unsteady blade pressures and acoustic recordings were sampled respectively at 20 kHz and 80 kHz. In order to isolate the harmonic noise of the tail rotor, these unsteady data have been post-processed using a time synchronous averaging based on the one-per-rev signal given by the trigger. This method, classically used for rotor harmonic noise analysis, reduces significantly the broadband noise. Moreover, since the tail rotor operates at a rotational speed which is not a multiple of the main rotor rotational speed, averaging acoustic data in the time domain on the tail rotor revolution period is also an effective way of isolating the tail rotor harmonic noise from the main rotor harmonic noise.

2 Computational method

2.1 Aerodynamic computations

The aerodynamic flow over the Dauphin helicopter in flight conditions is obtained by solving the URANS equations over the complete aircraft using the *elsA* structured CFD solver developed at ONERA and used for many years for helicopter applications [15].

2.1.1 Numerical method

The 3D compressible URANS equations are solved using the two equations k-ω turbulence model [16, 17] with the Zheng limiter [18, 19] and the corrections of Kok [20] and Menter [21]. The classical 2nd order centered scheme with scalar artificial viscosity [22] and Martinelli's correction [23] is used for the spatial discretisation. The numerical scheme is implicit in time. The time integration is discretized by a second-order upwind three-time-level formula which is solved by using a dual time stepping method [24]. For all cases, the time step used for computations corresponds to an azimuthal blade deplacement of 1 degree.

2.1.2 Geometry and computational grid

As can be seen in figure 4, describing the computed aircraft, the geometry has been simplified (lateral stabilizer removed, simplification of the engines fairing geometry). The main rotor is modeled using a non-uniform actuator disk method accounting for the load of the rotor over one revolution. It is included in a two cylindrical block mesh with about 17,000 cells. This steady state approximation of the main rotor reduces drastically the cost of the unsteady computation and allows densifying the computational grid in the Fenestron® area. The Navier-Stokes background grid contains 85 blocks and around 1.3 million of cells. The grid in the main part of the fuselage is a relatively coarse grid but it has been decided to limit the number of cells outside the Fenestron duct for CPU time consumption reasons.

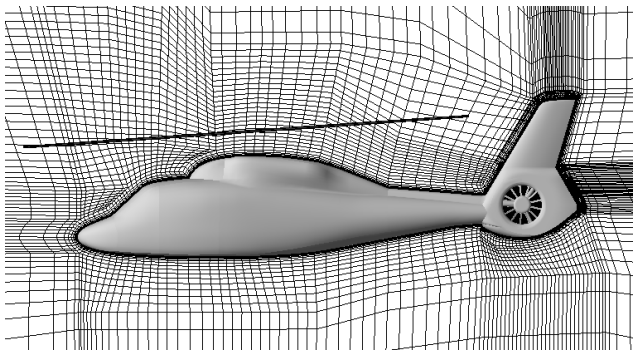

Figure 4: Helicopter simplified geometry, actuator disk location and computational grid for aerodynamic computations

As for the Fenestron® geometry, displayed in figure 5, it is fully discretized with a fixed part consisting in the duct, the 3 arms (the one containing the drive shaft larger than the others), the hub and a rotating part consisting in the 13 equally spaced blades with blade tip gaps. Each of the 13 Fenestron® blades is meshed with 3 blocks, which contain about 110,000 cells. The blade motion during the CFD computations is taken into account thanks to the Chimera method developed at ONERA [25] for helicopter configurations and consisting in the use of overlapping grids attached to the bodies in relative motion with respect to the aircraft (rotor blades as shown in figure 6). Interpolations are used to transfer the conservative and turbulent variables in the overlapping zone between the moving and fixed grids. The complete unsteady grid system contains 2.7 million cells.

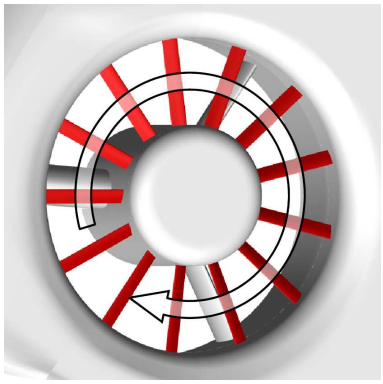

Figure 5: Fenestron® geometry used for CFD computations

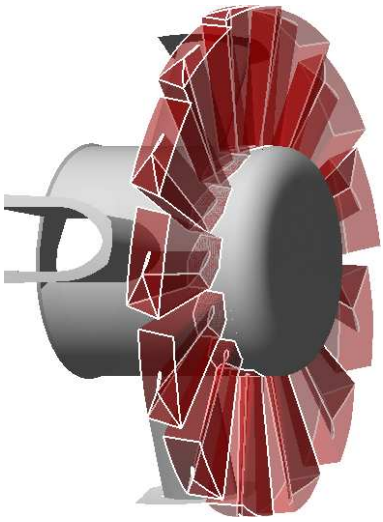

Figure 6: Chimera grids around rotating blades

2.2 Aeroacoustic computations

The aeroacoustic computations performed in this study have been carried out by solving the Ffowcs-Williams and Hawkings [26] (FW-H) equation formulated for porous surfaces. The radiated noise is computed by solving the FW-H equation in the time domain using the KIM solver [27] developed at ONERA.

For the acoustic computations presented in this paper, hypothesis is made that all acoustic sources are enclosed by the acoustic data surface so that the quadrupole term of the FW-H can be neglected. No influence of solid surfaces, nor of the inhomogeneous inflow is accounted for in the noise radiation computation. Furthermore, only discrete frequency noise is computed.

The porous acoustic data surfaces are sized and placed in such a way that they contain all acoustic sources of the Fenestron but also that they account for any reflexion or diffraction occuring in the shroud. These surfaces, displayed in figure 7, encompass the Fenestron® duct and are thus placed in an area where the flow is more homogenous than in the Fenestron® duct.

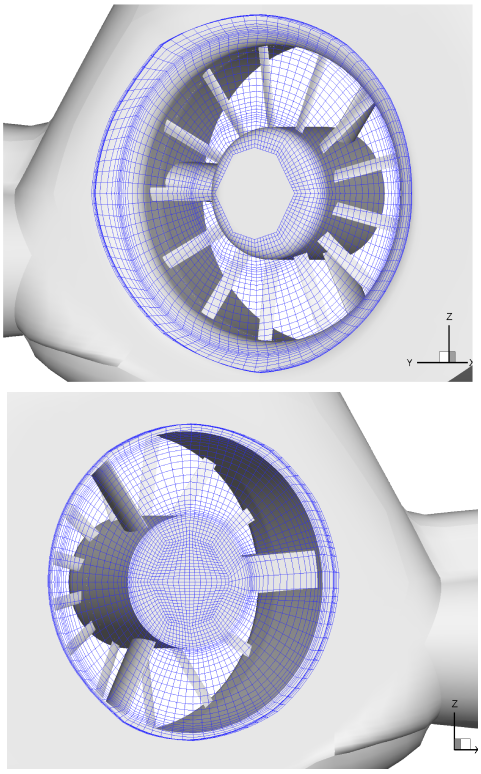

Figure 7: Porous surfaces at inflow (top) and outflow (bottom) sides for acoustic computations

3 Results and discussion

Two flight conditions, a takeoff at speed 75 kt and high climb speed 1500 ft/mn and a level flight at speed 150 kt, have been selected among the gathered data for numerical simulation.

For both flight conditions, the thrust provided by the Fenestron® in order to counterbalance the main rotor torque has been estimated with the HOST comprehensive code [28].

3.1 Takeoff flight

At takeoff condition, the thrust needed to counterbalance the main rotor torque is relatively high. Based on previous computations [1], the pitch angle of the Fenestron® blade is set to 22 degrees for the CFD computation. As can be seen in figure 8, the blade loading varies depending on the azimuth and the thrust is strong enough so that no flow separation occurs in the Fenestron® duct.

The measured and computed unsteady blade pressures at 0.7 R, displayed in figure 9, exhibit similar behavior over the complete rotation but the computation overestimates the pressure fluctuation at both suction and pressure sides. As a matter of fact, all flights were performed with some sideslip angle (about 2 degrees for the flight used for comparison) so that in real flight conditions a larger amount of the thrust needed to counterbalance the main rotor torque could be provided by the lift of the tail fin rather than by the Fenestron® itself. Since no experimental value of the Fenestron® thrust is available, there is no way to establish whether these discrepancies on the blade pressure level are related to the CFD modelization or to a mismatch between experimental and theoretical Fenestron® thrusts.

The spectra of the measured and computed acoustic pressure signals at experimental microphone locations are displayed in figure 10. The experimental and computed spectra exhibit similar shapes and the decrease of the tone levels with the frequency are in good agreement. The computed levels are overestimated with respect to the experiments but this has to be related with the unsteady blade pressure and thrust level issue discussed previously.

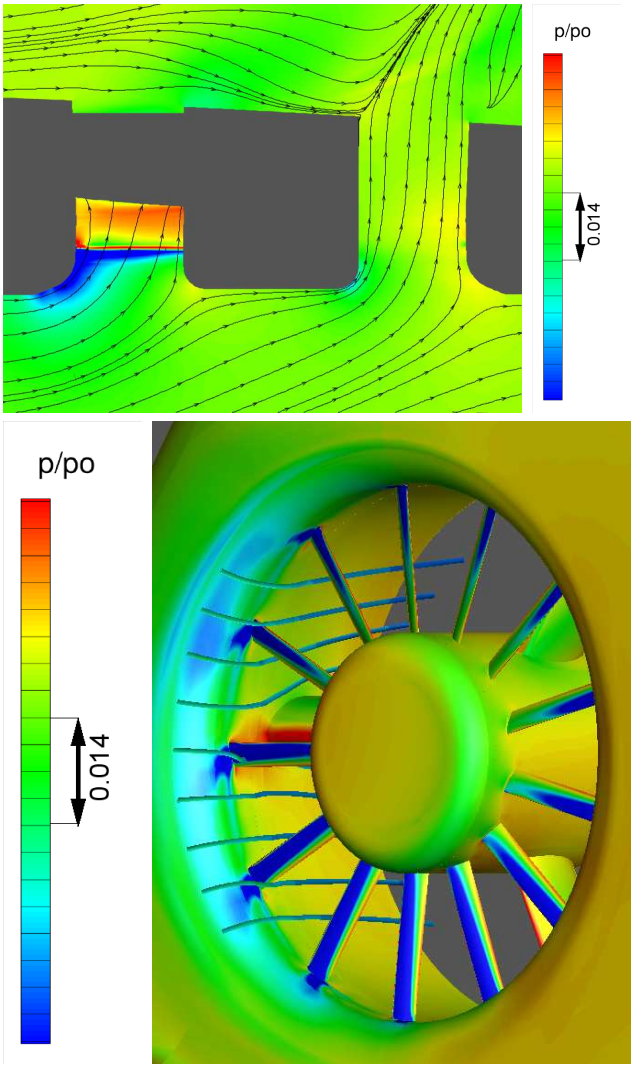

Figure 8: Computed streamlines and pressure field in the Fenestron® at takeoff condition, horizontal cut at mid-hub (top), blade skin and duct (bottom)

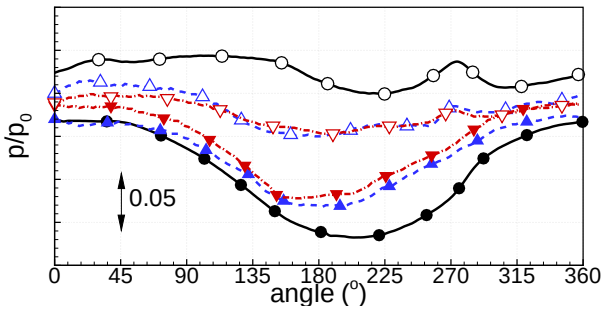

Figure 9: Time evolution of blade pressure on suction (●, ▼, ▲) and pressure (○, ▽, △) sides at 0.7 R: present computation (——), pressure on blade n°2 (- - -) and n°4 (- · -) for a test flight at speed 71.85 kt and climb speed 1488.25 ft/mn

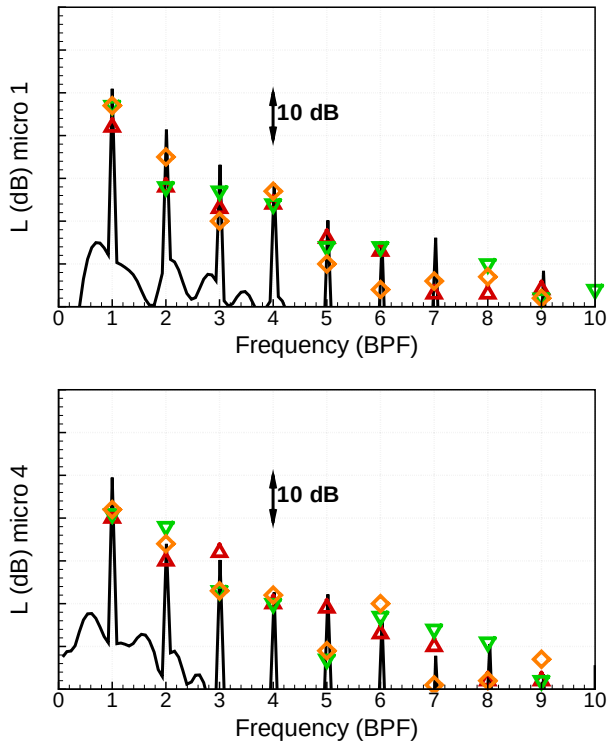

Figure 10: Spectra of the acoustic pressure at microphone 1 and 4 locations, respectively on port side and starboard, on the horizontal stabilizer: present computation (—), flight tests (◇, △, ▽) at speed varying between 71.85 and 75.85 kt and climb speed varying between 1488 and 1597 ft/mn

3.2 Level flight

For a level flight at speed 150 kt, a significant amount of the thrust needed to counterbalance the main rotor torque is provided by lift of the tail fin so that the thrust produced by the Fenestron® is much lower than for takeoff condition. The blade pitch angle used for the aerodynamic computation is thus set to 12 degrees. The higher flight speed put together with a lower thrust of the tail rotor result in a flow separation occuring in the upwind area of the Fenestron® intake, in front of the biggest hub support. It can be seen in figure 11 that this flow separation is attached to the wall over nearly half of the intake and alter significantly the flow in the blade tip crossing area. The time evolution of the measured and computed unsteady blade pressures at 0.7 R are displayed in figure 12. Experimental and computed pressures are in good agreement but just as for the takeoff flight condition the CFD solution overestimates the level of pressure fluctuation.

The spectra of the measured and computed acoustic signals are compared in figure 12. The agreement between experimental and computed values is good in terms of shape and trend of the tone level decrease but all the computed tone levels are underestimated with respect to the experiments except for the level at BPF for microphone n°1. As for the takeoff flight results, an experimental value of the Fenestron® thrust would be useful to improve the analysis of the discrepancies observed between the computations and the experiments.

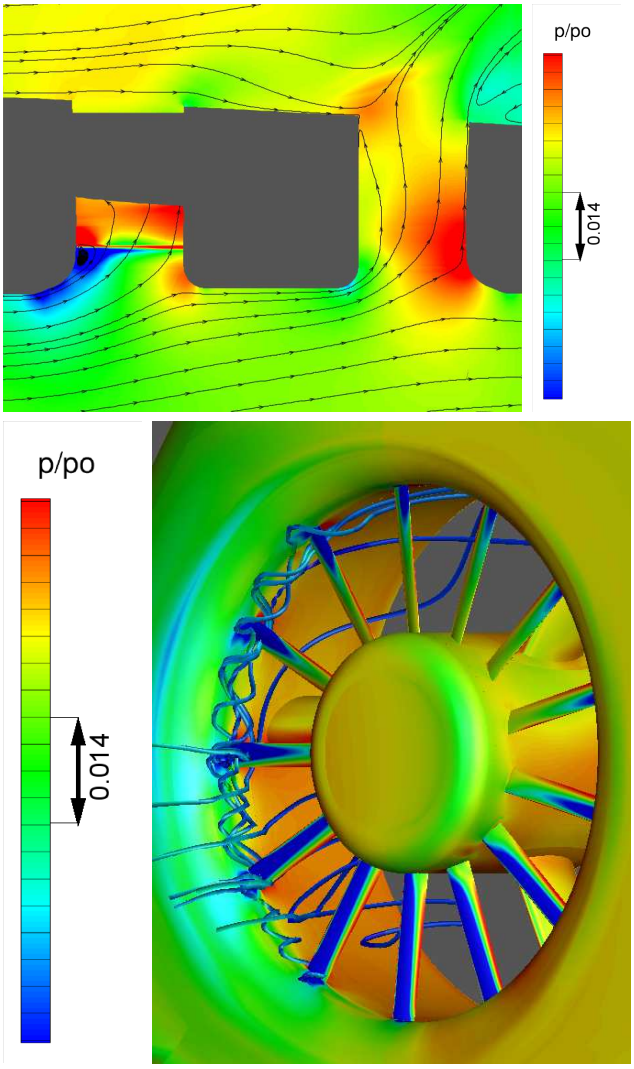

Figure 11: Computed streamlines and pressure field in the Fenestron® at level flight condition, horizontal cut at mid-hub (top), blade skin and duct (bottom)

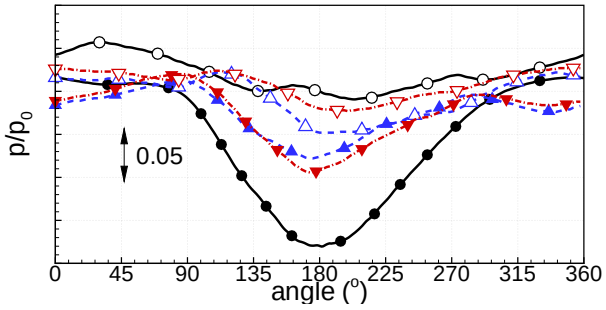

Figure 12: Time evolution of blade pressure on suction (●, ▼, ▲) and pressure (○, ▽, △) sides at 0.7 R: present computation (——), pressure on blade n°2 (- - -) and n°4 (- · -) for a test flight at speed 149.8 kt and climb speed 38.5 ft/mn

Conclusion and futur work

Aerodynamic and aeroacoustic computations of a Fenestron® fan-in-fin tail rotor have been compared against aerodynamic and acoustic flight test measurements. The experimental setup and test program aiming at the analysis of the aerodynamics and aeroacoustics of a Fenestron® tail rotor in real flight conditions have been presented. The *elsA* and KIM solvers used respectively to compute the aerodynamic flow over the full helicopter and the acoustic noise radiated by the Fenestron® have been described. Thanks to the use of overlapping grids (Chimera technique), unsteady viscous computations have been performed for two flight conditions: a takeoff at 75kt with high climb rate and a level flight at 150 kt.

For the takeoff flight condition, the Fenestron® thrust is high enough so that no flow separation occurs in the shroud while for the level flight at high speed the lower thrust combined with a higher forward speed result in a flow separation on the upwind part of the Fenestron® intake. For both flight conditions, the comparison of the measured and computed unsteady blade pressures over a revolution shows a good agreement but the CFD solution tends to overestimate the blade fluctuation. This indicates that the flow physics depending on the flight condition is captured by the CFD but also that the Fenestron® thrust used for CFD computations might be too high with respect to the experiments.

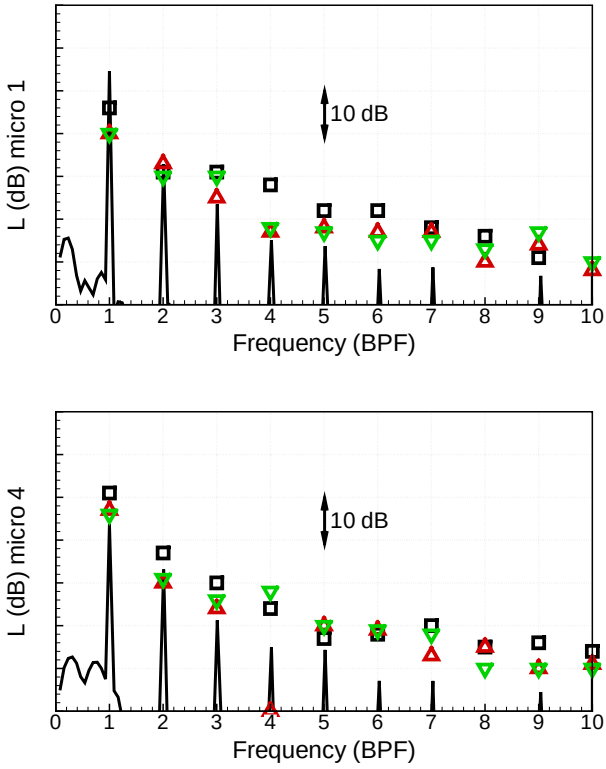

Figure 13: Spectra of the acoustic pressure at microphone 1 and 4 locations: present computation (——), flight tests (□, △, ▽) at speed varying between 146.78 and 149.75 kt and climb speed varying between 22 and 88 ft/mn

The acoustic computations have been carried out using the Ffowcs Williams-Hawkings porous surface approach to account for acoustic reflection in the Fenestron® duct. The spectra of the measured and computed acoustic signals at microphone locations exhibit similar shapes. The decrease rates of the tone levels with the frequency increase are also in good agreement but there are still significant discrepancies with regard to the tone levels.

A second flight test operation has been performed at the end of spring 2010 to measure noise footprints of some flight conditions selected for their interest in terms of acoustic nuisance, flow characteristics and certification concerns. For this new flight tests, the tail rotor torque has been measured in order to solve the issue related to the real thrust provided by the Fenestron® depending on the flight condition. The computational grid used for aerodynamic computations will also be refined

to enhance the accuracy of the unsteady flow field in the area encompassing the Fenestron® duct up to the porous surfaces used the acoustic computations.

Acknowledgments

The authors would like to thank the French Ministry of Civil Aviation (DGAC) for the financial support of this study. The authors would also like to recognize the efforts of all of the people involved in the test program from CEV, DeKerac company, Eurocopter and ONERA departments. We formulate a personal thank to Jean Prieur (DSNA) who made possible this study and retired before the flight tests. Finally we all have a very special thought to Frank Descatoire (DCSD) who worked from the very beginning of this program in the design, the development, the integration and testing of the instrumentation and who passed away just before the first flight.

References

[1] P. Gardarein, S. Canard, and J. Prieur. Unsteady aerodynamic and aeroacoustic simulations of a fenestron tail rotor. *62nd AHS Annual Forum*, Phoenix, USA, 2006.

[2] J. Prieur. Helicopter rotor aeroacoustic research at onera. *AHS Specialist's Meeting*, Seoul, Korea, 2007.

[3] L. Binet, D. Tristran, J.-C. Camus, L. Perthuis, and D. Pesenti. Innovative flight test instrumentation for in-flight noise measurement of a Dauphin's Fenestron. *35th ERF*, Hamburg, Germany, 2009.

[4] L. Binet, D. Tristran, J.-C. Camus, L. Perthuis, and D. Pesenti. Innovative instrumentation and flight tests for onboard aerodynamic and acoustic measurements of a Dauphin's Fenestron. *10th ONERA-DLR Aerospace Symposium*, Berlin, Germany, 2009.

[5] F. Falissard, P. Gardarein, and L. Binet. Aerodynamic and aeroacoustic results of the Fenestron noise flight test campaign. *10th ONERA-DLR Aerospace Symposium*, Berlin, Germany, 2009.

[6] L. Binet, F. Cuzieux, J.-C. Camus, and L. Perthuis. In-Flight and Ground Instrumentation for Dauphin's Fenestron Noise Investigation. *66th AHS Annual Forum*, Phoenix, USA, 2010.

[7] A. Vuillet and F. Morelli. Le fenestron sur hélicoptère. *19^{e} Colloque d'Aérodynamique Appliquée*, Marseille, France, 1982.

[8] M. Vialle and G. Arnaud. A new Generation of Fenestron Fan-in-Fin Tail Rotor on EC135. *19th ERF*, Cernobbio, Italy, 1993.

[9] M. Roger. Contrôle du bruit aérodynamique des machines tournantes axiales par modulation de pales. *Acustica*, 80:247–259, 1994.

[10] E. Mouterde, L. Sudre, A. M. Dequin, A. D'Alascio, and P. Haldenwang. Aerodynamic computation of isolated Fenestron® in hover conditions. *33rd ERF*, Kazan, Russia, 2007.

[11] A. D'Alascio, F. Le Chuiton, E. Mouterde, L. Sudre, S. Kirstein, and H.-P. Kau. Aerodynamic Study of the EC135 Fenestron® in Hovering Flight Conditions by means of CFD. *64th AHS Annual Forum*, Montréal, Canada, 2008.

[12] M. Kainz, F. Danner, H.-P. Kau, and F. Le Chuiton. Numerical investigation into the unsteady aerodynamics of a ducted helicopter tail rotor under side-wind conditions. *ASME Turbo Expo*, Glasgow, UK, 2010.

[13] D. Blacodon, G. Élias, D. Papillier, and J. Prieur. Noise source localization on a Dauphin helicopter in flight. *25th ERF*, Roma, Italy, 1999.

[14] D. Blacodon, G. Élias, J. Prieur, and D. Papillier. Noise source localization on a Dauphin helicopter in flight. *AHS J.*, 49(4):425–435, 2004.

[15] T. Renaud, C. Benoit, J.-C. Boniface, and P. Gardarein. Navier-Stokes Computations of a Complete Helicopter Configuration Accounting for Main and Tail Rotor Effects. *29th ERF*, Friedrichhafen, Germany, 2003.

[16] D. C. Wilcox. Reassessment of the Scale-Determining Equation ofr Advanced Turbulence Models. *AIAA J.*, 26:1299–1310, 1988.

[17] D. C. Wilcox. Simulation of Transition with a Two-Equation Turbulence Model. *AIAA J.*, 32:247–255, 1994.

[18] X. Zheng and F. Liu. Staggered upwind method for solving Navier-Stokes and k-ω turbulence model equations. *AIAA J.*, 33:991–998, 1995.

[19] F. Liu and X. Zheng. A strongly coupled time-marching method for solving the Navier-Stokes and k-ω turbulence model equations with multigrid. *J. Comput. Phys.*, 128:289–300, 1996.

[20] J. C. Kok. Resolving the Dependence on Freestream Values for the k-ω Turbulence Model. *AIAA J.*, 38:1292–1295, 2000.

[21] F. R. Menter. Zonal Two Equation (k-ω) Turbulence Models for Aerodynamic Flows. *AIAA Paper 93-2906*, 1993.

[22] A. Jameson, W. Schmidt, and E. Turkel. Numerical Solutions of the Euler Equations by Finite Volume Methods Using Runge-Kutta Time-Stepping Schemes. *AIAA Paper 81-1259*, 1981.

[23] L. Martinelli and A. Jameson. Validation of a Multigrid Method of the Reynolds Averaged Equations. *AIAA Paper 88-0414*, 1998.

[24] A. Jameson. Time dependent calculations using multigrid, with applications to unsteady flows past airfoils and wings. *AIAA Paper 91-1596*, 1991.

[25] C. Benoit, G. Jeanfaivre, and E. Canonne. Synthesis of ONERA Chimera method developed in the frame of CHANCE program. *31^{st} ERF*, Florence, Italy, 2005.

[26] J. E. Ffowcs Williams and D. L. Hawkings. Sound Generation by Turbulence and Surfaces in Arbitrary Motion. *Philo. Trans. Royal Society of London*, 264, A1151:321–342, 1969.

[27] J. Prieur and G. Rahier. Comparison of Ffowcs Williams-Hawkings and Kirchhoff rotor noise calculations. *AIAA Paper 98-2376*, 1998.

[28] B. Benoit, A.-M. Dequin, K. Kampa, W. Grunhagen, P.-M. Basset, and B. Gimonet. HOST: A General Helicopter Simulation Tool for Germany and France. *56^{th} AHS Annual Forum*, Virginia Beach, Virginia, 2000.